Sensors and Materials, Vol. 34, No. 4 (2022) 1367–1387
MYU Tokyo

S & M 2897

Water-cooling Radiator for CPU with Innovative Design: Experiments and Simulation

Hsin-Hung Lin,[1,2*] Zi-Hong Guo,[3] and Shu-Chun Chien[4]

[1]Department of Creative Product Design, Asia University, Taichung 41354, Taiwan
[2]Department of Medical Research, China Medical University Hospital, China Medical University, Taichung 406040, Taiwan
[3]Master Program of Hakka Cultural Industry, National Pingtung University, Pingtung 900391, Taiwan
[4]Department of Digital Media Design, Asia University, Taichung 41354, Taiwan

(Received July 5, 2021; accepted February 21, 2022)

Keywords: radiator fan, water-cooled thermal module, numerical simulation, experimental measurement, CPU radiator

A new water-cooling radiator is proposed for a CPU with an area of 28.7 mm^2 and a power of 100 W. The performance was of the radiator simulated with two different types of fan blades and compared with that of a conventional solid-cooling radiator. Then, the simulation results were validated through an experiment in which the temperature and thermal resistance of the radiator were measured at different fan and water pump speeds. The results showed that the thermal resistance of the water-cooling radiator was 0.073–0.15 °C/W at the maximum power of 100 W and a fan speed of 1000–3000 rpm. The proposed water-cooling radiator improves the cooling effect and has high efficiency. The heat dissipation of the CPU was improved with forward-inclined fan blades and the increased fan speed and water flow rate of the water-cooling system. The proposed water-cooling radiator with the fan blades is expected to improve the overall efficiency of CPUs and be applied to the manufacture of radiators for CPUs.

1. Introduction

With the rapidly improving performance of CPUs, researchers have put great effort into developing an appropriate heat management system for CPUs by researching their heat dissipation and airflow. The results have been applied to the design of CPUs to improve their performance.[1–3] The main focus of the design is to solve the problem caused by overheating and insufficient overall heat dissipation. For the heat management of the CPU radiator, the air temperature of the CPU module is monitored using thermal sensors.[4,5] The sensors play an important role in studying the heat dissipation of CPUs through accurate temperature measurement. Heat dissipation affects the performance of CPUs as an overheated CPU has reduced efficiency, which affects the overall performance of the computer. Thus, it is important to design a CPU module with good heat dissipation for normal operation.

Different designs have been proposed by researchers for optimized thermal management for the components of a computer. Whelan *et al.* designed a liquid-cooling system to reduce the

*Corresponding author: e-mail: hhlin@asia.edu.tw
https://doi.org/10.18494/SAM3531

ISSN 0914-4935

volume of a radiator that cooled a CPU of 200 W. The CPU's working temperature was 65 °C with a liquid temperature of 53 °C.[1] Choi *et al.* used the computational method of fluid dynamics to derive an appropriate design method for the radiator, which was verified by experiment and simulation. Their design reduced the thermal resistance of the radiator to 0.11−0.19 °C/W.[2] Pastukhov and Maydanik used heat pipes to reduce the thermal resistance of a radiator by 0.15−0.17 °C/W with an effective heat load of 1500 W.[3,6]

In general, the heat capacity for cooling a CPU exceeds 150 W.[3] Kim *et al.* studied the use of a micro-evaporation cycle of a cooler in a CPU. The design focused on the analysis of the latent heat of each cycle and the cooling effect of cooling fluid to improve the overall efficiency.[7] Liang and Hung added a U-shaped heat pipe to a high-frequency microprocessor and experimented with the air convection between and around the fins of a radiator with the heat pipe to calculate the heat transfer coefficient of the radiator.[5] The heat dissipation of the radiator was then optimized to minimize the thermal resistance of the U-shaped heat pipe.[5] Kim *et al.* proposed the design of a CPU radiator that changed the fan speed according to the cooling performance of an aluminum extrusion radiator. They observed that heat inside the radiator was effectively dissipated, thus cooling the CPU. The tolerable working temperature was 72–78 °C, and the power consumption of the heat source was 100 W at an ambient temperature of 22 °C.[7] Additional loop heat pipes increased heat dissipation and reduced the thermal resistance of the system to 0.29 °C/W at 180 W.[6] Naphon *et al.* applied micro-rectangular fins to a CPU and used deionized water as a cooling fluid. In their numerical study of fluid flow and heat transfer, the finite volume method (FVM) and the standard k–ε turbulence model were used to solve 3D control equations and describe the structure of the flow field. There was a reasonable correlation between the simulation and experimental results, and these results were used to improve the cooling performance and the system design of electronic equipment.[8] María *et al.* considered the pressure drop of a cooler as the optimization variable in designing a new water-cooling system to obtain the solution of a nonlinear mixed-integer problem.[9]

Previous studies attempted to reduce the thermal resistance of the water-cooling radiator by using a heat dissipation module. In general, the configuration and applicability of a water-cooling system obtained by simulation were compared with experimental results. However, the results do not provide a means of solving the heat problems of a CPU with a high temperature caused by high electric power consumption in existing systems. Because the heat deteriorates the characteristics and performance of the CPU, an effective method of cooling the CPU needs to be found and applied to the design of CPU cooling radiators.[10–12] Therefore, a new water-cooling radiator is proposed in this study to reduce the thermal resistance of CPUs. Experiments and simulations with the proposed radiator were carried out to investigate its effectiveness in managing the heat from a CPU. The results of this study are expected to provide an innovative design for a new thermal management system for the water-cooling radiator of a CPU.

2. System Configuration

The water-cooling radiator comprised a test box, heating element, temperature sensor, ambient temperature controller, and signal (Fig. 1).[13–15] A thermostat, OMRON PLC signal

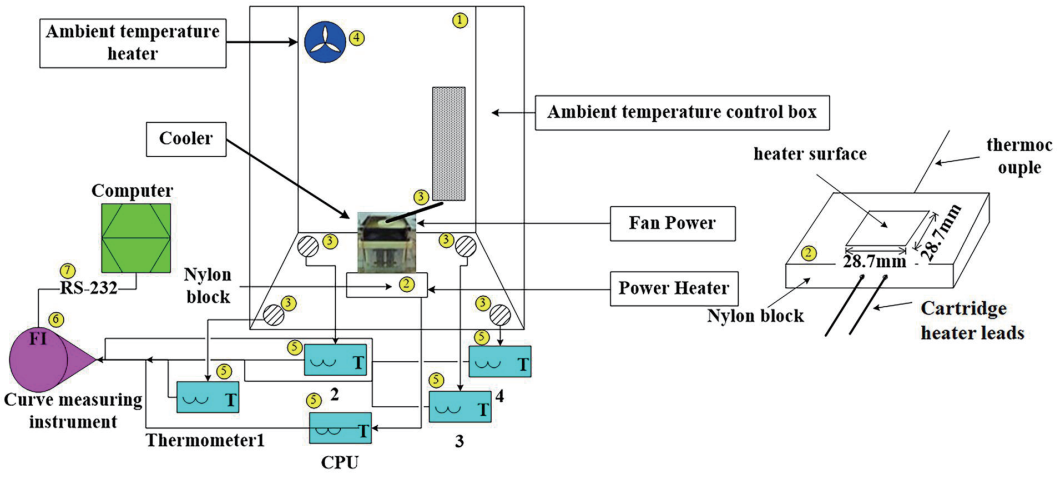

Fig. 1. (Color online) Radiator testing system and heating block diagram.

converter, RS-232 cable, and PC were used for the experiment. The test box was made of transparent acrylic sheets and an aluminum bottom to simulate the operating environment of a CPU of a desktop computer and observe the working condition in the test box.

2.1 Water-cooling and solid-cooling radiators

The dimensions of the water-cooling radiator are 95 mm × 95 mm × 50 mm ($l \times w \times h$). The internal components include the blades, motor, printed circuit board, fan frame, bracket, water pump, shunt sleeve, radiator body, and waterproof jacket. The heating element is located at the bottom of the radiator. To transfer the heat from the CPU, the pump circulates water to the fins to achieve convection and cooling. Figure 2 shows the circulating system of the water-cooling radiator.

Figure 3 shows the solid-cooling and water-cooling radiators with two different types of fan blades Q1 and Q2. The right side of Fig. 3(a) shows the structure of the water-cooling radiator. The center of the water-cooling radiator is hollow with water channels to reduce its weight and increase the area of the fins. The flow rate of the water pump can be increased to obtain high thermal conductivity. The solid-cooling radiator is heavier than the water-cooling radiator owing to its adoption of a conventional heat conduction module. The two radiators are compared to evaluate the efficiency of the water-cooling radiator in Fig. 3(a).[16] Then, the water-cooling radiator is simulated for the target heat of 100 W.

2.2 Fan blades

Two different types of fan blades are applied to the water-cooling radiator as shown in Fig. 4. The fans are designed by using the curve fitting method to obtain the 3D axial flow blades. Each type of fan blade has dimensions of 92 mm × 92 mm × 25 mm ($w \times l \times h$) and has different stagger and twist angles. A Q1 fan blade is forward inclined and has its air volume concentrated at the center, while a Q2 fan blade has a general plane shape with a scattered air volume.

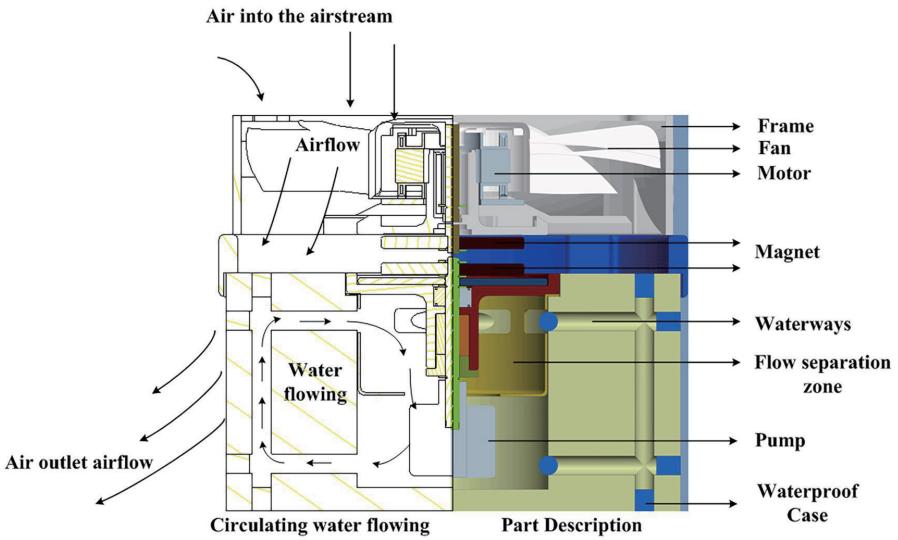

Fig. 2. (Color online) Water circulation of the water-cooling radiator. The left picture shows the air and water flow, and the right picture shows the parts of the radiator.

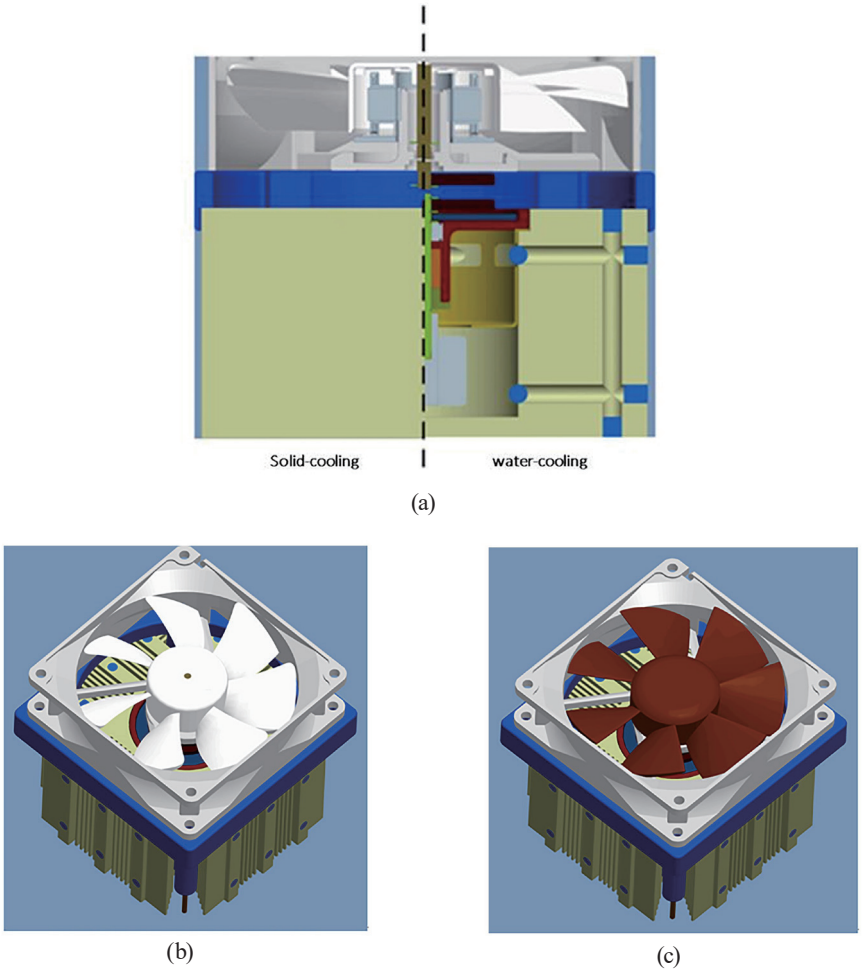

Fig. 3. (Color online) Water-cooling radiators with different fan blades. (a) Comparison of solid-cooling and water-cooling radiators. (b) Water-cooling radiator with Q1 fan blades. (c) Water-cooling radiator with Q2 fan blades.

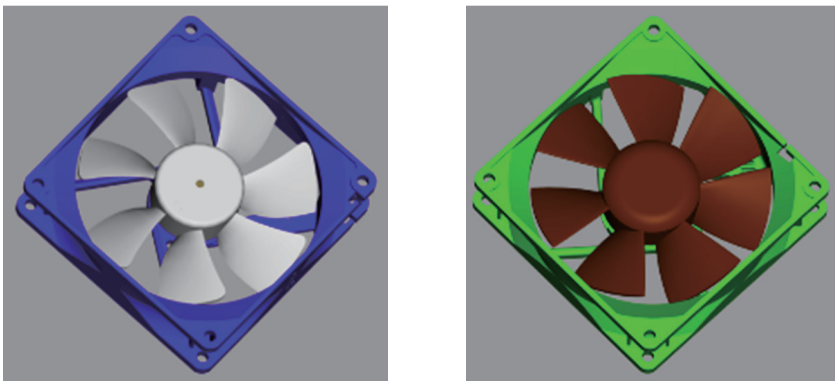

(a) (b)

Fig. 4. (Color online) Two different types of fan blades for the water-cooling radiator of the CPU. (a) Q1 fan model. (b) Q2 fan model.

3. Mathematical Models

The following mathematical models were used to reduce the complexity of the numerical simulation.[11]

Governing equations

Under 3D Cartesian coordinates, the governing equations for the experiment are defined as follows.

(1) Continuous equation

$$\frac{\partial u}{\partial x}+\frac{\partial v}{\partial y}+\frac{\partial w}{\partial z}=0 \tag{1}$$

(2) Momentum equation

x-direction:

$$\frac{\partial u}{\partial t}+\frac{\partial (u^2)}{\partial x}+\frac{\partial (uv)}{\partial y}+\frac{\partial (uw)}{\partial z}=-\frac{1}{\rho}\frac{\partial P}{\partial x}+v\left[\frac{\partial^2 u}{\partial x^2}+\frac{\partial^2 u}{\partial y^2}+\frac{\partial^2 u}{\partial z^2}\right] \tag{2}$$

y-direction:

$$\frac{\partial v}{\partial t}+\frac{\partial (uv)}{\partial x}+\frac{\partial (v^2)}{\partial y}+\frac{\partial (vw)}{\partial z}=-\frac{1}{\rho}\frac{\partial P}{\partial y}+v\left[\frac{\partial^2 u}{\partial x^2}+\frac{\partial^2 u}{\partial y^2}+\frac{\partial^2 u}{\partial z^2}\right] \tag{3}$$

z-direction:

$$\frac{\partial w}{\partial t}+\frac{\partial (uw)}{\partial x}+\frac{\partial (vw)}{\partial y}+\frac{\partial (w^2)}{\partial z}=-\frac{1}{\rho}\frac{\partial P}{\partial z}+v\left[\frac{\partial^2 w}{\partial x^2}+\frac{\partial^2 w}{\partial y^2}+\frac{\partial^2 w}{\partial z^2}\right] \tag{4}$$

(3) Energy equation

$$\frac{\partial T}{\partial t}+\frac{\partial (uT)}{\partial x}+\frac{\partial (vT)}{\partial y}+\frac{\partial (wT)}{\partial z}=\alpha(\frac{\partial^2 T}{\partial x^2}+\frac{\partial^2 T}{\partial y^2}+\frac{\partial^2 T}{\partial z^2})+\frac{q}{pC_P} \tag{5}$$

(4) The governing equation can be expressed by the following general formulas:

$$\frac{\partial (\rho\varphi)}{\partial t}+\frac{\partial (\rho\varphi u)}{\partial x}+\frac{\partial (\rho\varphi v)}{\partial y}+\frac{\partial (\rho\varphi w)}{\partial z}=\frac{\partial}{\partial x}\left(\Gamma\frac{\partial \varphi}{\partial x}\right)+\frac{\partial}{\partial y}\left(\Gamma\frac{\partial \varphi}{\partial y}\right)+\frac{\partial}{\partial z}\left(\Gamma\frac{\partial \varphi}{\partial z}\right)+s, \tag{6}$$

where $\frac{\partial (\rho\varphi u)}{\partial x}+\frac{\partial (\rho\varphi v)}{\partial y}+\frac{\partial (\rho\varphi w)}{\partial z}$ corresponds to convection, $\frac{\partial}{\partial x}\left(\Gamma\frac{\partial \varphi}{\partial x}\right)+\frac{\partial}{\partial y}\left(\Gamma\frac{\partial \varphi}{\partial y}\right)+\frac{\partial}{\partial z}\left(\Gamma\frac{\partial \varphi}{\partial z}\right)$ corresponds to diffusion, S is the source, $\frac{\partial (\rho\varphi)}{\partial t}$ corresponds to the unsteady state, φ represents the dependent variables, Γ is the diffusion coefficient corresponding to each dependent variable, and u, v, and w are the velocity components in the x-, y-, and z-directions, respectively. The independent variables that are compared with the dependent variable φ are described in Table 1.

In the FVM, computation is required for many small control volumes. Then, the equations of fluid mass, energy, and momentum can be converted into the algebraic equation[14]

$$\frac{\partial}{\partial t}\int_v (\rho\varphi)dV+\int_A \vec{n}\cdot\left(\rho\varphi\vec{V}\right)dA=\oint_A \vec{n}\cdot\left(\Gamma_\varphi\nabla\varphi\right)dA+\int_V S_\varphi\cdot dV, \tag{7}$$

where $\oint_A \vec{n}\cdot(\rho\varphi\vec{V})dA$ corresponds to convection, $\oint_A \vec{n}\cdot(\Gamma_\varphi\nabla\varphi)dA$ corresponds to diffusion, $\oint_V S_\varphi\cdot dV$ corresponds to the generation of heat, and $\frac{\partial}{\partial t}\int_v (\rho\varphi)dV$ corresponds to the unsteady state.

Table 1
Independent variables that are compared with the dependent variable of φ.

Continuity	*1*
x-momentum	*u*
y-momentum	*v*
z-momentum	*w*
Energy	*T*

Turbulence model theory

Turbulence makes the momentum, energy, and concentration of the fluid in each volume fluctuate at a high frequency in the FVM. Therefore, the simulation requires complex calculations. The control equations first need to be processed when simulating the turbulence to filter out the components of extremely high frequency or small size in the turbulence. The turbulence model requires known variables even though the modified equation contains unknown variables.

Standard k–ε turbulence model

The standard k–ε turbulence model is semi-empirical. The k–ε model is based on an equation for a completely turbulent flow field with molecular viscosity ignored. For the model, the transport equation is used to determine the turbulent kinetic energy (k) and dissipation rate (ε) of turbulent transport based on basic physical equations as follows.[14]

(1) Turbulent kinetic energy equation (k)

$$\frac{\partial}{\partial t}(\rho k)+\frac{\partial}{\partial x_i}(\rho k u_i)=\frac{\partial}{\partial x_j}\left[\left(\mu+\frac{\mu_t}{\sigma_k}\right)\frac{\partial k}{\partial x_j}\right]+G_k+G_b-\rho\varepsilon-Y_M \tag{8}$$

(2) Dissipation rate equation (ε)

$$\frac{\partial}{\partial t}(\rho\varepsilon)+\frac{\partial}{\partial x_i}(\rho\varepsilon u_i)=\frac{\partial}{\partial x_j}\left[\left(\mu+\frac{\mu_t}{\sigma_\varepsilon}\right)\frac{\partial \varepsilon}{\partial x_j}\right]+C_{1s}\frac{\varepsilon}{k}(G_k+C_{3\varepsilon}G_b)-C_{2g\rho}\frac{\varepsilon^2}{k} \tag{9}$$

(3) Turbulent viscosity coefficient (μ_t)

$$\mu_t=\rho C_\mu\frac{k^2}{\varepsilon} \tag{10}$$

In these equations, G_k represents the turbulent kinetic energy generated by the laminar flow velocity gradient, G_b the turbulent kinetic energy generated by the buoyant force, and Y_M the fluctuation generated by excessive diffusion in the compressible turbulence. σ_k and σ_ε are turbulent Prandtl numbers of turbulent kinetic energy and dissipation, respectively. $C_{1\varepsilon}$, $C_{2\varepsilon}$, and $C_{3\varepsilon}$ are empirical constants whose suggested values are shown in Table 2.

Table 2
Constant coefficients of standard k–ε turbulence model.

$C_{1\varepsilon}$	$C_{2\varepsilon}$	C_μ	C_k	$C_{3\varepsilon}$
1.44	1.92	0.09	1.0	1.3

Power dissipation theory of CPU

Figure 5 shows the boundary of the insulated heat exchange system. The heat exchange capacity of the system is equal to that of the heater. The relationship between the heat exchange capacity and the inlet and outlet of the working fluid is expressed as[17]

$$\dot{Q}_{ex} = \dot{m}c_p(T_0 - T_i) = \dot{m}(h_0 - h_1) = \dot{Q}_{Heater}. \tag{11}$$

The heat exchange capacity is also expressed by the internal and external temperature differences of the radiator. The overall heat transfer coefficient (U) and heat transfer area (A) are related by the following equation:

$$\dot{Q}_{ex} = UA(T_{Heater.avg} - T_{l,avg}), \tag{12}$$

where Q is the heat flux (kW), $\dot{m}$ is the mass flow rate (kg/s), c_p is the specific heat (kJ/kg°C), T is the temperature (°C), h is the enthalpy (kJ/kg), U is the overall heat transfer coefficient (kW/m^2°C), A is the area (m^2), and l, ex, i, and o represent liquid, heat exchange, inlet, and outlet, respectively.

The heat transfer area of the heater and the fixed flow rate of the working fluid are fixed, and the average temperature of the working fluid of the radiator is close to the average surface temperature of the bottom plate. This indicates that the heat exchange system has a high heat transfer coefficient. Therefore, the similar surface temperature of the radiator to that of the working fluid indicates that the heat exchange system has a higher heat dissipation than the radiator's bottom plate under the test conditions.

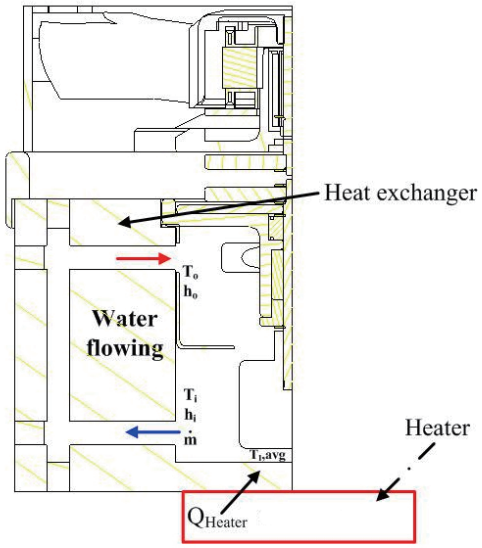

Fig. 5. (Color online) Schematic diagram of the heat exchange system.

4. Simulation Parameters

4.1 Simulation of fan

Grid setting

The grid of the fan (Fig. 6) is divided into three main areas: the inlet flow, fan flow, and outlet flow channels. The total number of grid points is 1.97 million and the total number of grids is 2.65 million. The inlet and outlet grids of the fan model are respectively established to analyze the up- and downstream flow fields of the fan and determine the boundary conditions. In the area close to the main flow channel, densification is required to meet the inlet and outlet boundary conditions of the flow field. Since there is no other impedance, the grid setting in the inlet and outlet areas must have a sufficiently wide range to satisfy the actual operating conditions. The blade wheel is redesigned according to the blade shape. After the flow field of the fan is simulated, the blade shape is modified on the basis of the analysis results to improve the performance. After that, the different blades are installed on the newly designed wheels. The flow field of the blades is simulated again to investigate the effect of the axial flow on the flow field and overall performance. Finally, the effect of the two different types of fan blades is simulated to correct the fan blade wheel.[18,19]

Water-cooling radiator model

The water-cooling radiator model used for simulation is illustrated in Fig. 7. The following design parameters are necessary for the simulation to evaluate the efficiency of water circulation in the water-cooling radiator. The model has a circular waterway of 2.5 mm diameter and a circulation volume of 27.5 mm^3 for the simulation of the water circulation rate. The number of grids and the convergence time decrease owing to the simplified internal structure. The

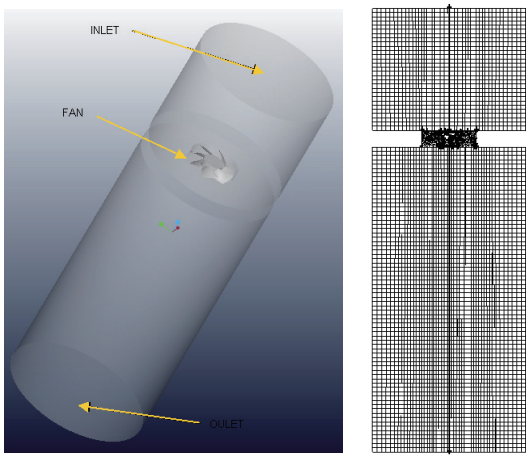

(a) (b)

Fig. 6. (Color online) Fan grid distribution. (a) Numerical model structure of the fan. (b) Section structure of the grid.

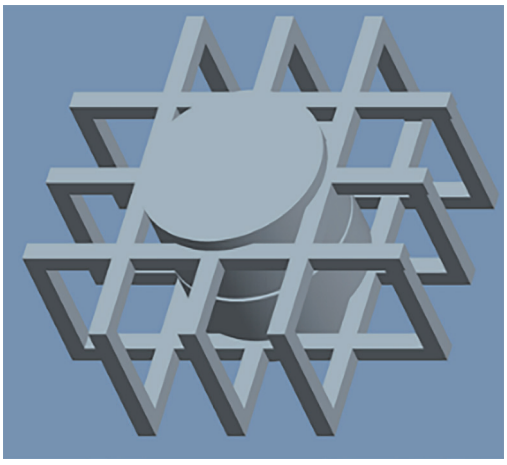

Fig. 7. (Color online) Model of water-cooling radiator.

circulating water is compressed by the water pump to generate an appropriate flow rate and passes through 12 channels in the circulating waterway. The water flows out from the upper outlet as the water pressure increases. Therefore, the heat is transferred to the upper fin by the water and dissipated by the airflow of the fan.

4.2 Simulation of radiator

Figure 8 shows the model for simulating the water-cooling radiator. The radiator is placed at a position one-third of the way from the center to the top. For simulation, it is assumed that there is an airflow inlet and walls on four sides and an airflow outlet at the bottom.

Boundary conditions

The boundary conditions of the inlet, outlet, and a wall are described in Table 3. The simulation is carried out for different values of the airflow of the fan, water flow, and temperature. When the radiator is heated, its geometry becomes complicated. Thus, the setting and calculation steps are established as follows.

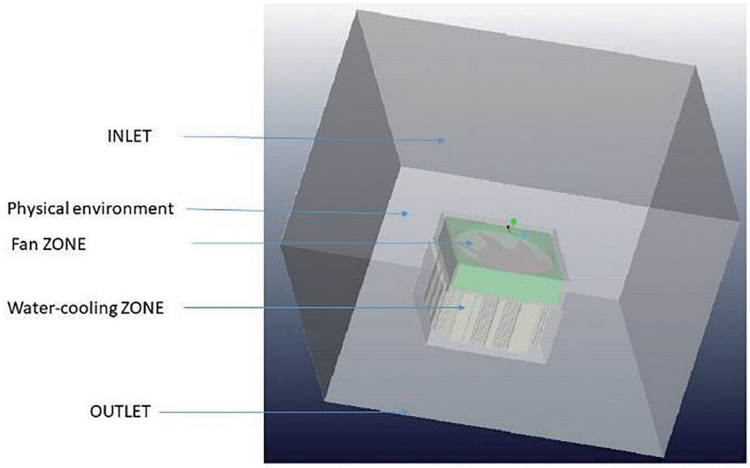

Fig. 8. (Color online) Model of water-cooling circulation.

Table 3
Boundary conditions when simulating the water-cooling radiator.

Boundary condition	Description
Inlet	For the initial calculation to simulate a fan in infinite space, a normal atmospheric pressure P_0 is set.
Outlet	The atmospheric space at the outlet generates airflow by fan flow to the outside, so a normal atmospheric pressure P_0 is adopted as the outlet boundary condition.
Wall	The fluid flowing through the wall must meet the requirement of impenetrability as well as no-slip condition. Regardless of the thermal radiation effect and ambient temperature, 25 °C is set. The turbulence model is established together with vortex flow correction. In the fluid rotation of the Markov random field model, the rotational speed is set as 1500, 2000, 2500, and 3000 rpm. The heat source at the chip position is set as 100 W.

(1) Set the fan flow rate, inlet, outlet, speed, pressure, and fan fluid properties.
(2) Set the properties of the water pump, water pump speed, and relaxation coefficient.
(3) Set the temperature, define the energy equation, and solve the temperature field equation.

Grid setting

The water-cooling radiator used for simulation consists of a water pump, circulating water channels, radiator body, fan body, and system grids. The total number of grid points of the system is 1.01 million and the total number of grids is 1.03 million as shown in Fig. 9. The water speed is reduced to less than 0.2 m/s to ensure the circulation ability of the water-cooling radiator. The air volume of the fan must be limited to 20 ft^3/min (cfm) on the basis of the system capacity. In accordance with the overall thermal conductivity, a fan size of 50 mm × 92 mm ($l \times w$) is selected. The water speed is fixed at 0.2 m/s. All the parameters are selected to reduce the radiator's volume and its total heat capacity.[20]

5. Simulation

5.1 Airflow rate of fan blades

The airflow rate is compared for the Q1 and Q2 fan blades. Rotational speeds of 1500, 2000, 2500, and 3000 rpm are used for comparison as shown in Fig. 10. The air pressure of Q1 at 1500 rpm (Q1-FAN-1500RPM) is 1.844 mmAq and the air volume is 34.05 cfm, while those for Q2 (Q2-FAN-1500RPM) are 1.68 mmAq and 32.45 cfm. The calculated air flow rates at 2000 rpm are 45.4 cfm for Q1 (Q1-FAN-2000RPM) and 41.3 cfm for Q2 (Q2-FAN-2000RPM). The air volume of Q2 at the rotational speed of 2000 rpm is lower than that of Q1. These results are used for the simulation and comparison of the radiators.

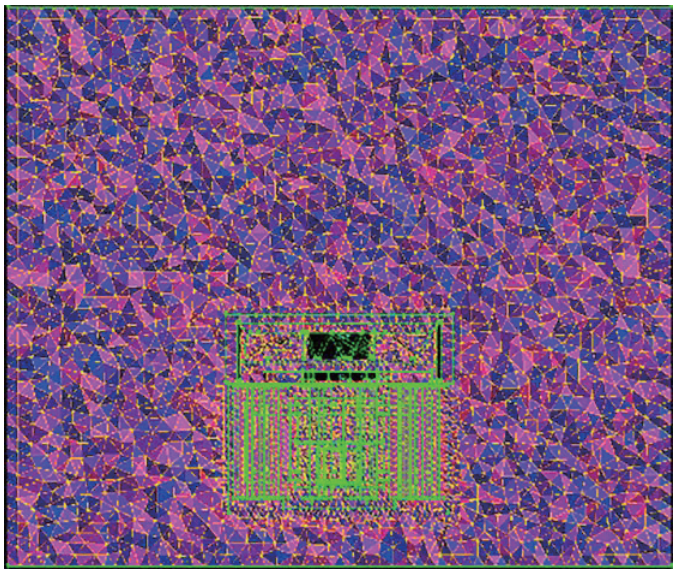

Fig. 9. (Color online) Grids of the water-cooling radiator.

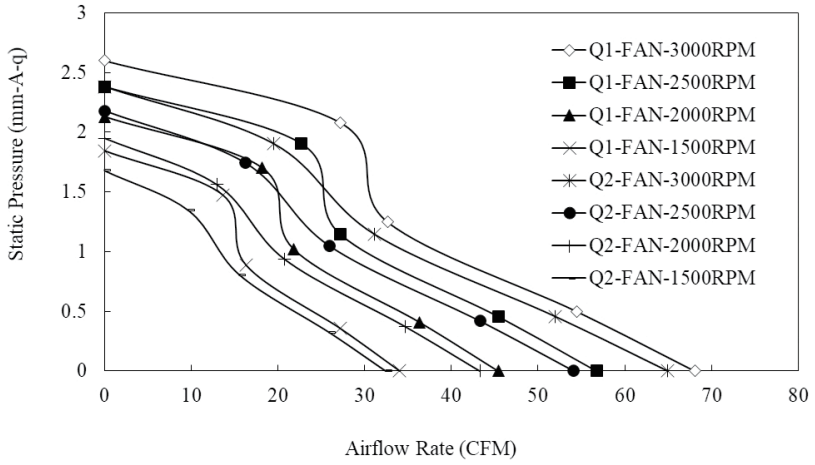

Fig. 10. Comparison of airflow rate and static pressure for Q1 and Q2.

5.2 Water circulation of radiator

The parameters of the water circulation affected the flow field simulation. For the subsequent analysis of the simulation results, it is necessary to define the relative positions of the heat flow. In the analysis of the flow field, the direction of the inlet velocity is set perpendicular to the x–z plane. The speed diagram of the flow field between the heat dissipation module and the fin is presented in Fig. 11(b). A high flow rate of water in the channels causes the pressure on the pump to increase.

The water flows along the axial direction (y–z) of the inlet from the bottom, then radially out of the channel (Fig. 12). The pressure is created by the heat and by the water pump and makes the water circulate owing to the increase in kinetic energy. As a result, the circulating water achieves the required pressure and speed, which are 12.4–20.8 mmAq and 1500–2000 rpm, respectively. The results of the experiment will help to optimize the water-cooling radiator.

6. Results and Discussion

6.1 Simulation results

Effect of fan blades

The simulation was carried out for the Q1 and Q2 fan blades for the water-cooling and solid-cooling radiators. Figures 13(a) and 13(b) show that the heat produced by the CPU is transferred to the fin through water circulation and then to the external flow field by forced convection. Figures 13(c)–13(f) present a comparison of the speed and pressure distributions of the water- and solid-cooling radiators. According to the temperature distribution of the fin, the temperature of the water-cooling radiator is lower than that of the solid-cooling radiator. This results in the more even distribution of the fin temperature in the water-cooling radiator than in the solid-cooling radiator. When the heat is transferred from the CPU to the aluminum bottom of the

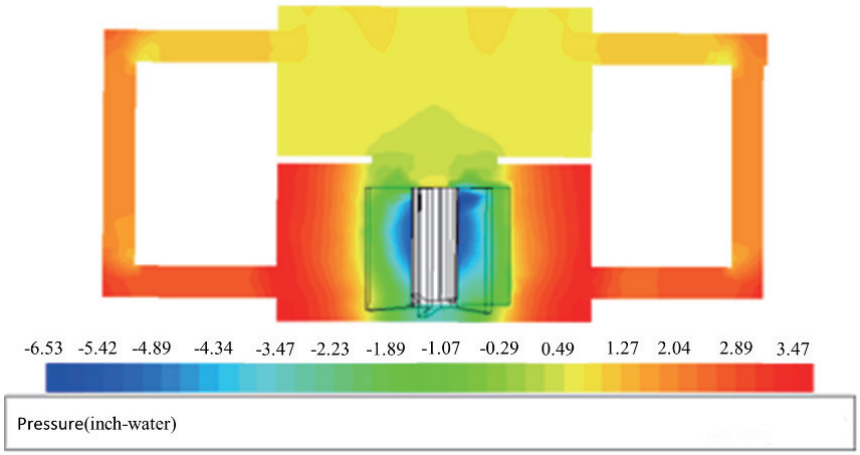

(a)

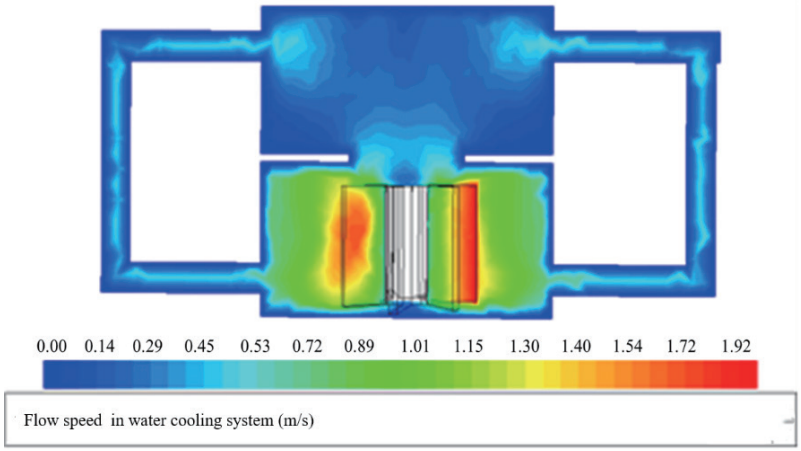

(b)

Fig. 11. (Color online) Distributions of (a) pressure and (b) speed of the water channel in the water-cooling radiator.

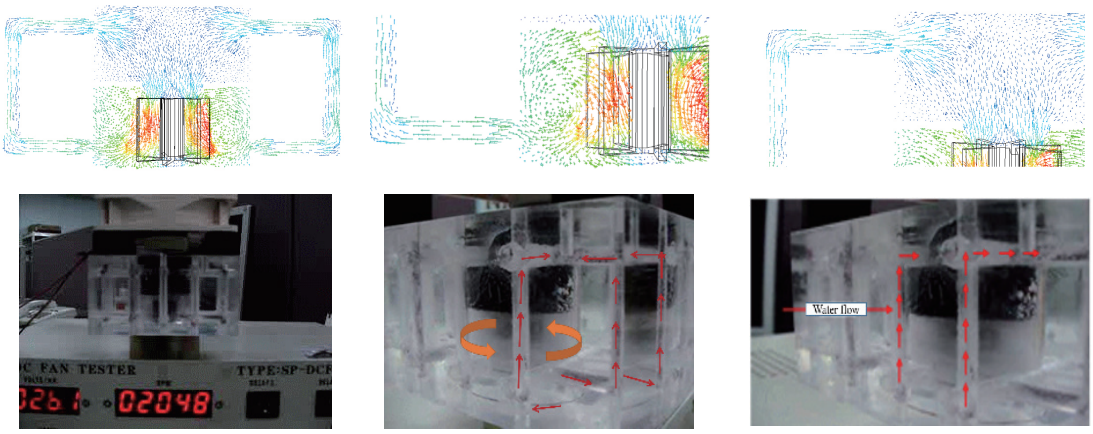

(a) (b) (c)

Fig. 12. (Color online) Simulation results of the water circulation system. (a) Pump speed. (b) Water flow rate. (c) Water flow direction.

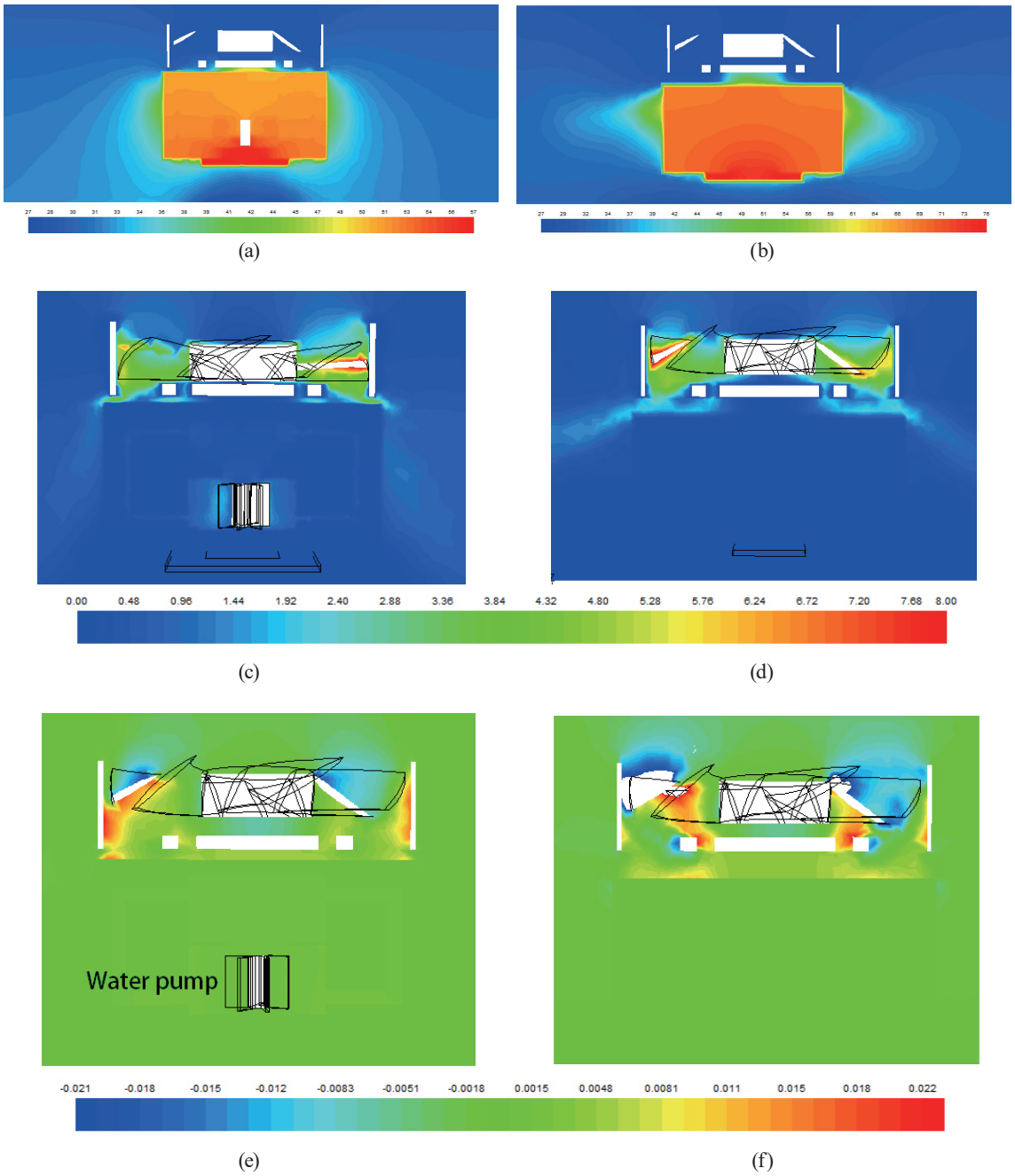

Fig. 13. (Color online) Distributions of (a, b) static temperature (°C), (c, d) speed (m/s), and (e, f) static pressure (inches-water) of the water-cooling and solid-cooling radiators. (a) Temperature distribution of the water-cooling radiator. (b) Temperature distribution of the solid-cooling radiator. (c) Speed distribution of the water-cooling radiator. (d) Speed distribution of the solid-cooling radiator. (e) Pressure distribution of the water-cooling radiator. (f) Pressure distribution of the solid-cooling radiator.

system, the thermal impedance decreases owing to the high thermal conductivity of the aluminum. Then, the heat is quickly transferred to the fin to maintain the temperature of the CPU in the ideal range.

The effects of the surface temperature of the fin, heat convection, and heat exchange must be determined for the simulation. When the heat flux increases, the temperature difference increases, but the effect of heat convection on the temperature difference is not significant. The parameters affecting the heat dissipation of the water-cooling radiator include the heat convection and conduction coefficients. Comparing the surface temperature with the water temperature helps clarify the correlation between the temperature difference and the thermal resistance. During the measurement of the surface temperature of the fin, the heat flux remains unchanged. The lower the average surface temperature, the greater the heat convection coefficient. Also, the greater the heat conduction coefficient, the smaller the thermal resistance and surface temperature difference. Thus, the average surface temperature and the surface temperature difference are required to estimate the thermal resistance.

Table 4 presents the results of the simulation for different blade types and rotational speeds of the fan. The radiators show the lowest temperatures for M4CP (Q1) and M8CP (Q2) (9.84 and 13.2 ℃ for the water-cooling and solid-cooling radiators, respectively) at the rotational speed of 3000 rpm, which provided the strongest airflow. The largest temperature differences of 16.8 and 17.8 ℃ are observed in M4CP (Q1) and M7CP (Q1) at 3000 and 2500 rpm, respectively. For M1CP (Q1) and M5CP (Q2), the different fans on the same radiator have a temperature difference of about 0.2 ℃. The results in Table 4 show that Q1 in the water-cooling radiator is more efficient for lowering the temperature than Q2 in the solid-cooling radiator.

Effect of fan speed on thermal resistance

Thermal resistance R_{ca} is defined as

$$R_{ca} = \frac{(T_c - T_a)}{w}, \tag{13}$$

where T_c is the surface temperature of the CPU, T_a is the ambient temperature (the arithmetic mean of the measured air inlet temperature of the fan), P is the CPU's designed thermal power, and W is the heat load.

Table 4
Comparison of simulation results of the water-cooling and solid-cooling radiators at 100 W.

Simulation code	Blade type	Rotational speed (rpm)	Temperature difference (℃)			
			Water-cooling radiator	Solid-cooling radiator	ΔT (%)	ΔT (℃)
M1CP	Q1 fan blade	1500	39.3	52.3	75.14	13.0
M2CP		2000	27.3	40.7	67.08	13.4
M3CP		2500	15.2	30.1	50.50	14.9
M4CP		3000	9.84	26.6	36.99	16.8
M5CP	Q2 fan blade	1500	43.1	56.3	76.55	13.2
M6CP		2000	31.2	46.3	67.39	15.1
M7CP		2500	19.5	37.3	52.28	17.8
M8CP		3000	13.2	29.3	45.05	16.1

Figure 14 shows the changes in the thermal resistance of the radiators with the fan speed. The water-cooling radiator shows a lower thermal resistance than the solid-cooling radiator regardless of the fan type. The figure also shows the thermal behavior of the radiators. The results indicate that the heat from the CPU is transferred to the radiator effectively in the water-cooling radiator. Moreover, the radiator at the heat load of 100 W has a thermal resistance of 0.073–0.15 °C/W at 30 °C.

The thermal resistance is used to evaluate the performance of the radiator. The performance of the fin is considered to be stable with a 3D heat flow. The heat transfer rate η from the fin to the surroundings is calculated using Eq. (17) from the heat loads with Q1 and Q2 given by Eqs. (14)–(16). Since the water-cooling radiator has a symmetrical structure (the two radiator bodies have the same transfer efficiency), each half of the structure is assumed to be the same heat source. Figure 15 shows that the heat transfer rate decreases with increasing fan speed. This relationship implies that a higher fan speed has a more efficient cooling effect, causing the heat transfer rate to decrease, even though a lower fan speed results in the system having a higher temperature (Table 4).

$$Q_1 = mCp\Delta T_1 \tag{14}$$

$$Q_2 = mCp\Delta T_2 \tag{15}$$

$$\Delta Q = m_1 Cp\Delta T_1 \tag{16}$$

$$\eta_1 = \frac{\Delta Q_1}{Qin} \times 100\% \tag{17}$$

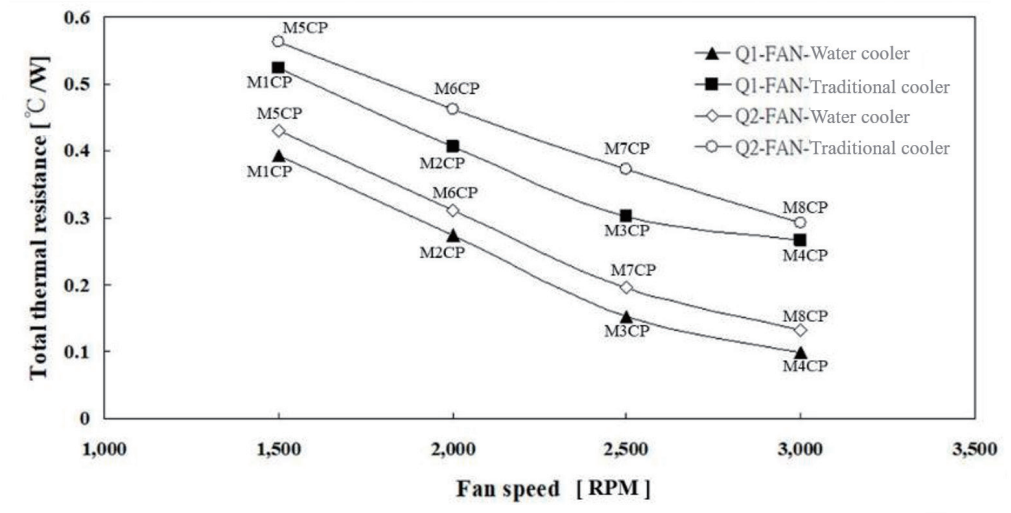

Fig. 14. Simulation results of thermal resistance with a heat load of 100 W and an ambient temperature of 30 °C.

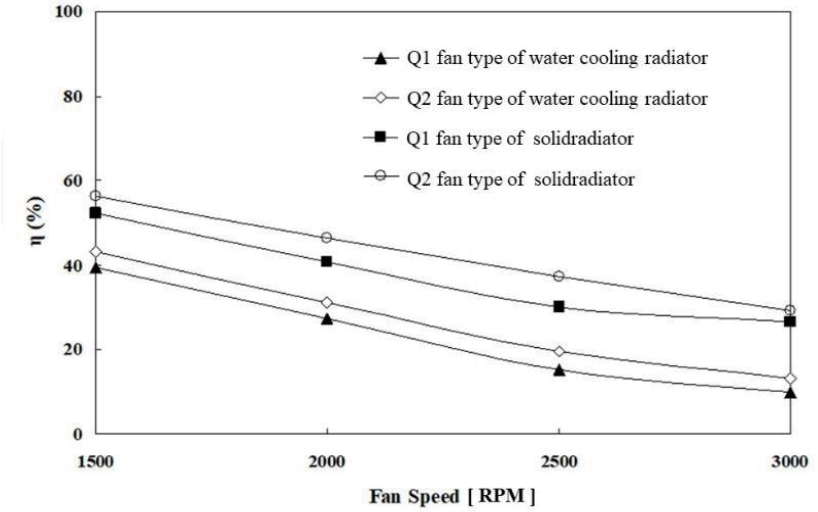

Fig. 15. Heat transfer rates of the water-cooling and solid-cooling radiators.

Pump speed

Figures 16(a) and 16(b) respectively show that the pump speed and water flow rate affect the water temperature at the inlet and outlet. This indicates that the higher the pump speed and water flow rate, the lower the temperature. The fan blade type also affects the water temperature, as discussed previously (Table 4). Figure 16(c) presents simulation results revealing that a higher fan speed decreases the thermal resistance significantly. The radiator has better performance with Q1 than with Q2, with the thermal resistance 10% lower on average for Q1. The radiator with Q1 achieves the best thermal resistance of 0.1 °C/W at 3000 rpm. A simulated thermal resistance of lower than 0.1 °C/W is thought to be sufficient for the normal operation of the CPU.

6.2 Experimental results

An experiment was carried out to compare the results obtained using a real radiator with those from the simulation. The efficiency of heat dissipation of the water-cooling radiator was also compared with that of the solid-cooling radiator. Parameters such as the grid density and the number of iterations, and the properties of the materials in the simulation model may be different from those in the experiment. Therefore, the input parameters for the experiment must be adjusted by considering the simulation results. In the experiment, the heat dissipation efficiency for the water-cooling radiator was measured at a heat load of 100 W with forced convection by Q1 and Q2. The temperature of the CPU was also measured in a closed system. The ambient temperature in the closed system increased monotonically owing to the heat from the CPU. Figure 17 shows the water-cooling radiator used in the experiment.

Figure 18 shows the thermal resistance of the water-cooling radiator with Q1 and Q2 at various fan speeds. Increasing the rotational speed of the fan decreases the thermal resistance. This implies that the water circulation transfers the heat to the fin efficiently and accelerates the heat transfer. The heat transfer disperses the heat load. In the case of forced convection by the

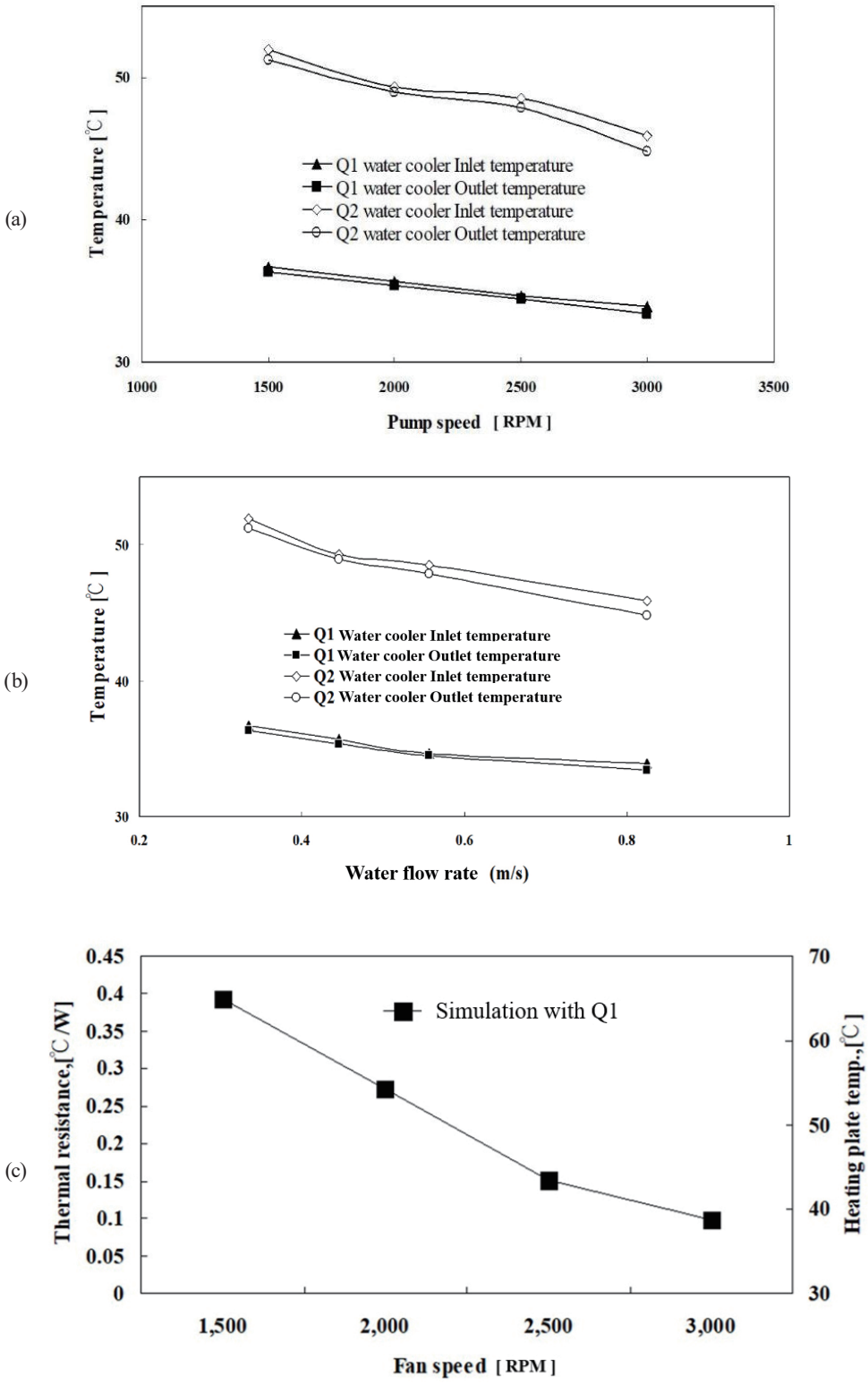

Fig. 16. (a) and (b) Temperature changes and (c) thermal resistance as functions of pump speed, water flow rate, and fan speed, respectively, at the water inlet and outlet. (a) Changes in water temperature at inlet and outlet with pump speed. (b) Changes in water temperature at inlet and outlet with water flow rate. (c) Changes in thermal resistance with fan speed.

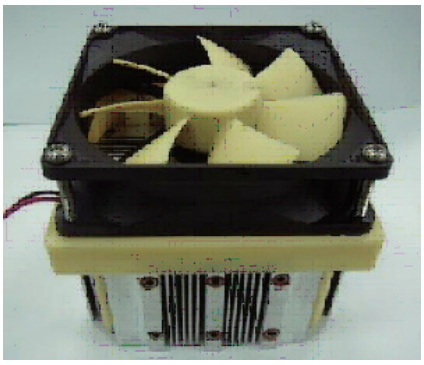

Fig. 17. (Color online) Water-cooling radiator used in the experiment.

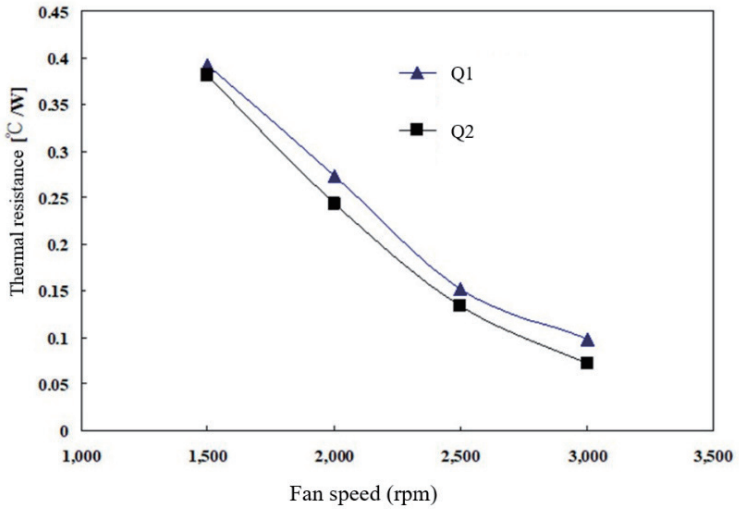

Fig. 18. Effect of the rotational speed of the fan on the thermal resistance.

fan, the thermal resistance was calculated as 0.09−0.1℃/W at the heat load of 100 W. The experiment was performed at rotational speeds of 1500, 2000, 2500, and 3000 rpm. The thermal resistances obtained from the experiment and simulation were close to 0.1 ℃/W at 3000 rpm and the heat load of 100 W. The water-cooling radiator showed a difference of 9.8% in the temperature between the simulation and experiment results, demonstrating the accuracy of the simulation results (Fig. 18).

7. Conclusions

The cooling effect of a water-cooling radiator was analyzed through simulation and experiment. The difference in cooling efficiency between fan blades Q1 and Q2 was 5−8% and the volume of the circulating air was 3−7 cfm. The efficiency was higher and the volume of the circulating air was larger for Q1 than for Q2. The simulation results showed that the thermal resistance of the water-cooling radiator was 0.073–0.15 ℃/W and improved by 15−30%

compared with that of the solid-cooling radiator. The water circulation dissipated the heat from the CPU efficiently. The difference in temperature between the water-cooling and solid-cooling radiators after heat dispersion was 16 °C, meaning that the thermal efficiency of the water-cooling radiator was increased by 30%. According to the results, the proposed water-cooling radiator provides effective thermal management for CPU cooling, and its design can be applied to the manufacture of radiators to enhance the performance of computers.

References

1 B. P. Whelan, R. Kempers, and A. J. Robinson: Appl. Therm. Eng. **39** (2012) 86. https://doi.org/10.1016/j.applthermaleng.2012.01.013
2 J. Choi, M. Jeong, J. Yoo, and M. Seo: Appl. Therm. Eng. **44** (2012) 50. https://doi.org/10.1016/j.applthermaleng.2012.03.027
3 V. G. Pastukhov and Y. F. Maydanik: Appl. Therm. Eng. **29** (2009) 3140. https://doi.org/10.1016/j.applthermaleng.2009.04.016
4 J. B. Marcinichen, J. R. Thome, and B. Michel: Int. J. Refrig. **33** (2010) 1264. https://doi.org/10.1016/j.ijrefrig.2010.06.008
5 T. S. Liang and Y. M. Hung: Energy Convers. Manag. **51** (2010) 2109. https://doi.org/10.1016/j.enconman.2010.03.003
6 V. G. Pastukhov and Y. F. Maydanik: Appl. Therm. Eng. **27** (2007) 894. https://doi.org/10.1016/j.applthermaleng.2006.09.003
7 K. S. Kim, M. H. Won, J. W. Kim, and B. J. Back: Appl. Therm. Eng. **23** (2003) 1137. https://doi.org/10.1016/S1359-4311(03)00044-9
8 P. Naphon, S. Klangchart, and S. Wongwises: Int. Commun. Heat. Mass. **36** (2009) 834. https://doi.org/10.1016/j.icheatmasstransfer.2009.06.010
9 P. O. J. María, S. G. Medardo, and J. G. Arturo: Comput. Chem. Eng. **34** (2010) 177. https://doi.org/10.1016/j.compchemeng.2009.07.006
10 L. Y. Jeng and T. P. Teng: Exp. Therm. Fluid. Sci. **45** (2013) 155. https://doi.org/10.1016/j.expthermflusci.2012.10.020
11 S. M. H. Hashemi, S. A. Fazeli, H. Zirakzadeh, and M. Ashjaee: Int. Commun. Heat. Mass. **39** (2012) 877. https://doi.org/10.1016/j.icheatmasstransfer.2012.04.005
12 Y. Tekin and O. E. Ataer: Int. J. Refrig. **33** (2010) 12. https://doi.org/10.1016/j.ijrefrig.2009.08.011
13 K. T. Chiang: Appl. Therm. Eng. **27** (2007) 2473. https://doi.org/10.1016/j.applthermaleng.2007.02.004
14 H. A. Mohammed, P. Gunnasegaran, and N. H. Shuaib: Int. Commun. Heat. Mass. **37** (2010) 1496. https://doi.org/10.1016/j.icheatmasstransfer.2010.08.020
15 L. Y. Jeng and T. P. Teng: Exp. Therm. Fluid. Sci. **45** (2013) 155. https://doi.org/10.1016/j.expthermflusci.2012.10.020
16 C. N. Hsu and Y. L. Tsai: Sens. Mater. **32** (2020) 4299. https://doi.org/10.18494/SAM.2020.3143
17 Q. J. Wang, Z. H. Wang, J. L. Zhou, and S. Dong: Sens. Mater. **32** (2020) 3867. https://doi.org/10.18494/SAM.2020.2942
18 Y. Nakajima, T. Kawase, R. Suzuki, T. Sugino, S. Onogi, K. Kawashima, and K. Ouchi: Sens. Mater. **33** (2021) 1703. https://doi.org/10.18494/SAM.2021.3333
19 J. Liao, H. Yu, J. Yan, and S. H. Hsu: Sens. Mater. **33** (2021) 1645. https://doi.org/10.18494/SAM.2021.3180
20 C. Cheng: Sens. Mater. **33** (2021) 3269. https://doi.org/10.18494/SAM.2021.3385

About the Authors

Hsin-Hung Lin is a professor in the Department of Creative Product Design, Asia University, Taichung, Taiwan. His major research interests include the application of fuzzy set theory in product design, concurrent engineering in product design, computer-aided design, the application of neural networks and gray theory in product design, color planning for product design, heat transfer analysis, and the application of reverse engineering in product design. (hhlin@asia.edu.tw)

Zi-Hong Guo is a professor in the Master Program of Hakka Cultural Industry, National Pingtung University, Pingtung, Taiwan. His major research interests include the application of entrepreneurship management, strategy, and social media marketing. (morgan@mail.nptu.edu.tw)

Shu-Chun Chien is currently a Ph.D. candidate at the Department of Digital Media Design, Asia University, Taichung, Taiwan. Her major research interests include ceramic design, product design, design management, and fine arts. (kristi.chien@gmail.com)